Pesticide Biochemistry and Physiology 200 (2024) 105814

Contents lists available at ScienceDirect

Pesticide Biochemistry and Physiology

journal homepage: www.elsevier.com/locate/pest

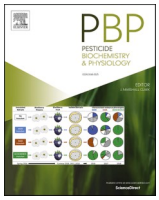

Indole alkaloids isolated from the *Nicotiana tabacum*-derived *Aspergillus fumigatus* 0338 as potential inhibitors for tobacco powdery mildew and their mode of actions

Yue-Yu Ma [a,b], Gui Pu [a], Hua-Yin Liu [a], Sui Yao [a], Guang-Hui Kong [c], Yu-Ping Wu [c], Yin-Ke Li [b,c], Wei-Guang Wang [b], Min Zhou [b], Qiu-Fen Hu [a,b,*], Feng-Xian Yang [a,b,*]

[a] *Key Laboratory of Chemistry in Ethnic Medicinal Resources, State Ethnic Affairs Commission & Ministry of Education, Yunnan Minzu University, Kunming 650500, PR China*

[b] *Key Laboratory of Tropical Plant Resource and Sustainable Use, Xishuangbanna Tropical Botanical Garden, Chinese Academy of Sciences, Kunming 650223, PR China*

[c] *Yunnan Academy of Tobacco Agricultural Sciences, Kunming 650031, PR China*

ARTICLE INFO

Keywords:
Aspergillus fumigatus
Indole alkaloid derivatives
Golovinomyces cichoracearum
Anti-*G. Cichoracearum* activity
Tobacco powdery mildew

ABSTRACT

To explore active natural products against tobacco powdery mildew caused by *Golovinomyces cichoracearum*, an extract from the fermentation of endophytic *Aspergillus fumigatus* 0338 was investigated. The mechanisms of action for active compounds were also studied in detail. As a result, 14 indole alkaloid derivatives were isolated, with seven being newly discovered (**1**–**7**) and the remaining seven previously described (**8**–**14**). Notably, compounds **1**–**3** are rare linearly fused 6/6/5 tricyclic prenylated indole alkaloids, with asperversiamide J being the only known natural product of this kind. The isopentenyl substitutions at the 5-position in compounds **4** and **5** are also rare, with only compounds 1-(5-prenyl-1*H*-indol-3-yl)-propan-2-one (**8**) and 1-(6-methoxy-5-prenyl-1*H*-indol3-yl)-propan-2-one currently available. In addition, compounds **6** and **7** are new framework indole alkaloid derivatives bearing a 6-methyl-1,7-dihydro-2*H*-azepin-2-one ring. The purified compounds were evaluated for their activity against *G. cichoracearum*, and the results revealed that compounds **7** and **9** demonstrated obvious anti-*G. cichoracearum* activities with an inhibition rate of 82.6% and 85.2%, respectively, at a concentration of 250 μg/mL, these rates were better than that of the positive control agent, carbendazim (78.6%). The protective and curative effects of compounds **7** and **9** were also better than that of positive control, at the same concentration. Moreover, the mechanistic study showed that treatment with compound **9** significantly increased the structural tightness of tobacco leaves and directly affect the conidiospores of *G. cichoracearum*, thereby enhancing resistance. Compounds **7** and **9** could also induce systemic acquired resistance (SAR), directly regulating the expression of defense enzymes, defense genes, and plant semaphorins, which may further contribute to increased plant resistance. Based on the activity experiments and molecular dockings, the indole core structure may be the foundation of these compounds' anti-*G. cichoracearum* activity. Among them, the indole derivative parent structures of compounds **6**, **7**, and **9** exhibit strong effects. Moreover, the methoxy substitution in compound **7** can enhance their activity. By isolating and structurally identifying the above indole alkaloids, new candidates for anti-powdery mildew chemical screening were discovered, which could enhance the utilization of *N. tabacum*-derived fungi in pesticide development.

1. Introduction

Tobacco powdery mildew is a foliar disease induced by *G. cichoracearum*, a biotrophic parasitic pathogen within the subphylum Ascomycota, which detrimentally affects mature leaves, spreading from lower to upper foliage (Gullner et al., 2017; Yang et al., 2023b). This plant pathogenic fungus is primarily disseminated via airflow and exhibits a broad host spectrum, with a short incubation period and a high incidence rate (Glawe, 2008). It causes significant economic losses in tobacco cultivation due to its negative impact on yield and quality (Xing

* Corresponding authors at: Key Laboratory of Chemistry in Ethnic Medicinal Resources, State Ethnic Affairs Commission & Ministry of Education, Yunnan Minzu University, Kunming 650500, PR China.

E-mail addresses: huqf_tg@163.com (Q.-F. Hu), yangfengxian90@163.com (F.-X. Yang).

https://doi.org/10.1016/j.pestbp.2024.105814
Received 14 December 2023; Received in revised form 2 February 2024; Accepted 3 February 2024
Available online 8 February 2024

et al., 2015). Infected leaves, exhibiting a dark brown color, distinct spot lesions, reduced elasticity, and diminished aroma, are prone to breakage and possess inferior industrial usability, ultimately compromising their overall quality.

Tobacco is an important cash crop in China, and it is easy to contract powdery mildew. To date, powdery mildew has been mainly controlled by chemical fungicides such as triazole, benzimidazole, organic sulfur, and methoxyacrylate (Gullner et al., 2017; Wang et al., 2012b; Yang et al., 2023b). Compared to synthetic antifungal chemicals, using natural products are a very promising preventive strategy, characterized by low toxicity and no residual effects (Basaid et al., 2020; Jiménez-Reyes et al., 2019). The various secondary metabolites secreted by endophytic fungi can protect plants from pests and pathogens (Degenkolb and Vilcinskas, 2016; Shi et al., 2020) or serve as crop growth promoters (Gamit et al., 2023).

Among the myriad of endophytic fungi, *Aspergillus* species are renowned as abundant, valuable sources of natural products, encompassing a wide range of chemical classes with fascinating biological activities (Hagag et al., 2022; Jiao et al., 2018; Yang et al., 2023a). In our prior research, we identified bioactive metabolites, such as alkaloids (Dai et al., 2023; Yang et al., 2022), butyrolactones (Zhou et al., 2015a; Zhou et al., 2015b), isocoumarins (Zhou et al., 2016), anthraquinones (Dai et al., 2022). Indole alkaloids, a group of naturally occurring phytochemicals, are renowned for their diverse biological activities (Liu et al., 2020b; Singh and Singh, 2018; Tabassum et al., 2021), and have been widely studied due to their significant inhibitory effects on various DNA, RNA viruses and phytopathogens (Abookleesh et al., 2022; Guo et al., 2020b; Kong et al., 2023). We isolated *A. fumigatus* 0338 from the stem of cigar tobacco samples. During small-scale fermentation, we utilized an HPLC-UV/vis diode array detector and noticed that the extract of this strain had distinctive UV absorption associated with indole alkaloids, similar to those previously identified in our laboratory (Kong et al., 2023). To discover more indole alkaloids with anti-*G. cichoracearum* activity, larger-scale fermentation led to the successful isolation of seven new (**1**–**7**), as well as seven known (**8**–**14**) indole alkaloid derivatives (Fig. 1). As *A. fumigatus* is a pathogenic bacterium and a prohibited strain in agriculture (Barber et al., 2020), we have sterilized all instruments and spaces used after obtaining the fermentation crude extract in our study to prevent the dissemination of this fungal strain. This manuscript presents comprehensive details regarding the isolation, structure elucidation, and activities of these compounds against tobacco powdery mildew.

2. Materials and methods

2.1. General procedures for the isolation and identification of compounds

UV and IR (KBr) spectra were acquired using a UV-1900 spectrophotometer (Shimadzu, Kyoto, Japan) and a FTS185 spectrophotometer (Bio-Rad, California, USA), respectively. Nuclear Magnetic Resonance (NMR) experiments were conducted using a Bruker DRX-500 NMR spectrometer (Bruker, Karlsruhe, Germany) with tetramethylsilane (TMS) serving as the internal standard. ESIMS and HRESIMS analyses were carried out using a 6540 Q-TOF mass spectrometer coupled with an Agilent 1290 UPLC system (Agilent Technologies, Wilmington, DE, USA). For normal column chromatography (CC), we utilized Silica gel with a mesh size of 80–100 or 200–300 (Qingdao Marine Chemical, Inc., Qingdao, China). Fractions was monitored using thin-layer chromatography (TLC) plates (Qingdao Marine Chemical, Inc., Qingdao, China). The visualization of spots was achieved by heating the silica gel plates at around 120 °C following the application of a 5% bismuth potassium iodide solution. An Agilent 1260 (Agilent Technologies, Wilmington, DE, USA) semi-preparative liquid chromatography system was used for semi-preparative HPLC with Venusil MP C18 columns (5 μm, 10 mm ×

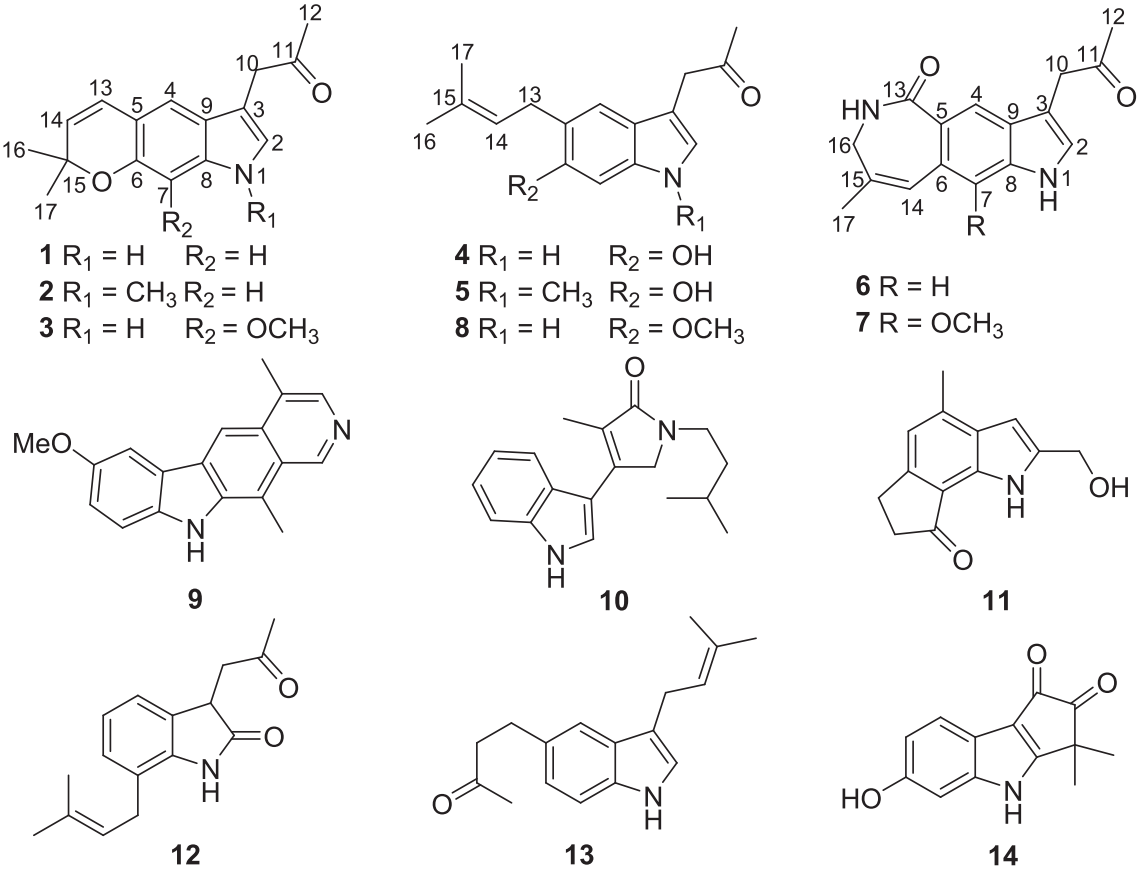

Fig. 1. Structures of compounds **1**–**14**.

250 mm, Bonna-Agela, Tianjin, China) or Zorbax PrepHT GF C18 columns (5 μm, 9.4 mm × 250 mm, Agilent, Palo Alto, USA).

2.2. Biological material

The *A. fumigatus* 0338 was isolated from the stem of cigar tobacco (a variety of *N. tabacum*), collected from Tengchong Prefecture, Yunnan Province in 2020. The identification of the strain was performed by Dr. Feng-Xian Yang, one of the authors, using BLAST analysis of the ribosomal internal transcribed spacer (ITS) sequence (GenBank No. OQ244321) available in the NCBI database. This strain is preserved in the Key Laboratory of Ethnic Medicine Resource Chemistry, Yunnan Minzu University.

2.3. Fermentation of A. fumigatus 0338

The strain was grown on potato dextrose agar at 27 °C for 7 days. Agar plugs were inoculated into 250 mL Erlenmeyer flasks containing 100 mL of potato dextrose broth. The flasks were placed on a rotary shaker set at 180 rpm at 27 °C for 7 days. Large-scale fermentation was conducted in a 1.0 L Fernbach flask filled with 300 g of rice, 300 g of perlite, and 100 g of purified water. The pH of the solution was adjusted to 6.5 before autoclaving. Each flask was inoculated with 5.0 mL of seed culture and incubated at 27 °C for 30 days. 100 Fernbach flasks were used in this study.

2.4. Extraction and purification

The solid fermentation products underwent extraction using 70% aqueous Me_2CO (4 × 20 L), followed by filtration and concentration under reduced pressure until Me_2CO was completely removed. Subsequently, the obtained extract underwent three extractions using EtOAc, resulting in an EtOAc extract weighing 69.2 g. The crude extract was further purified using CC (SiO_2) with stepwise elution using a gradient system of $CHCl_3$/MeOH (20:1, 8:2, 7:3, 6:4, and 5:5, *v*/v), resulting in the separation of five fractions, namely A–E. Fraction B (Fr·B, 17.6 g) was then subjected to silica gel CC with $CHCl_3$/Me_2CO (10:0, 9:1, 8:2, 7:3, 6:4, and 5:5, v/v) as the mobile phase, affording six subfractions (Fr·B1–Fr·B6). Fr·B2 (9,1, 2.85 g) underwent silica gel CC (200–300 mesh) followed by semi-preparative HPLC separation using a solvent mixture of 69% methanol/water at a flow rate of 3 mL/min. This process resulted in the isolation of compounds **4** (22.7 mg), **5** (20.4 mg), **6** (19.2 mg), and **7** (25.8 mg). Fr·B3 (8,2, 3.06 g) was subjected to silica gel CC (200–300 mesh). The resulting fraction was further purified using semi-preparative HPLC with a solvent mixture of 60% methanol/water at a flow rate of 3 mL/min. This purification process yielded compounds **1** (18.6 mg), **2** (18.2 mg), **3** (29.7 mg), **9** (18.4 mg), **10** (23.6 mg), and **11** (17.2 mg). Fr·B4 (7,3, 2.67 g) underwent additional purification using silica gel CC (200–300 mesh) and semi-preparative HPLC (55% methanol/water, 3 mL/min), resulting in the separation of compounds **8** (30.4 mg), **12** (19.7 mg), **13** (21.3 mg) and **14** (20.5 mg).

Asperfumigatone A (1) obtained as a pale yellow gum; UV (MeOH) λ_{max} (log ε) 218 (3.96), 285 (3.79), 332 (3.68) nm; IR (KBr) ν_{max} 3379, 3064, 2976, 1684, 1620, 1558, 1482, 1369, 1277, 1165, 1063, 839 cm^{-1}; ^1H NMR and ^{13}C NMR data ($CDCl_3$, 500 and 125 MHz), see Table 1; positive ESIMS *m/z* 278 $[M + Na]^+$; positive HRESIMS *m/z* 278.1165 $[M + Na]^+$ (calcd for $C_{16}H_{17}NNaO_2$, 278.1157).

Asperfumigatone B (2) obtained as a pale yellow gum; UV (MeOH) λ_{max} (log ε) 218 (3.92), 288 (3.68), 335 (3.64) nm; IR (KBr) ν_{max} 3070, 2982, 1680, 1614, 1543, 1475, 1364, 1284, 1148, 1059, 865 cm^{-1}; ^1H NMR and ^{13}C NMR data ($CDCl_3$, 500 and 125 MHz), see Table 1; positive ESIMS *m/z* 292 $[M + Na]^+$; positive HRESIMS *m/z* 292.1325 $[M + Na]^+$ (calcd for $C_{17}H_{19}NNaO_2$, 292.1313).

Asperfumigatone C (3) obtained as a pale yellow gum; UV (MeOH) λ_{max} (log ε) 218 (3.96), 285 (3.79), 332 (3.68) nm; IR (KBr) ν_{max} 3370, 3058, 2979, 1682, 1616, 1564, 1473, 1375, 1268, 1182, 1146, 1067, 816 cm^{-1}; ^1H NMR and ^{13}C NMR data ($CDCl_3$, 500 and 125 MHz), see Table 1; positive ESIMS *m/z* 308 $[M + Na]^+$; positive HRESIMS *m/z* 308.1270 $[M + Na]^+$ (calcd for $C_{17}H_{19}NaO_3$, 308.1263).

Asperfumigatone D (4) obtained as a pale yellow gum; UV (MeOH) λ_{max} (log ε) 215 (3.84), 270 (3.63), 318 (3.55) nm; IR (KBr) ν_{max} 3408, 3374, 3062, 2928, 1686, 1622, 1549, 1468, 1338, 1280, 1169, 1054, 852 cm^{-1}; ^1H NMR and ^{13}C NMR data ($CDCl_3$, 500 and 125 MHz), see Table 1; positive ESIMS *m/z* 280 $[M + Na]^+$; positive HRESIMS *m/z* 280.1318 $[M + Na]^+$ (calcd for $C_{16}H_{19}NaO_2$, 280.1313).

Asperfumigatone E (5) obtained as a pale yellow gum; UV (MeOH) λ_{max} (log ε) 215 (3.87), 272 (3.68), 320 (3.59) nm; IR (KBr) ν_{max} 3408, 3065, 2972, 1681, 1622, 1560, 1465, 1357, 1286, 1169, 1046, 848 cm^{-1}; ^1H NMR and ^{13}C NMR data ($CDCl_3$, 500 and 125 MHz), see Table 1; positive ESIMS *m/z* 294 $[M + Na]^+$; positive HRESIMS *m/z* 294.1462 $[M + Na]^+$ (calcd for $C_{16}H_{19}NNaO$, 294.1470).

Asperfumigatone F (6) obtained as a pale yellow gum; UV (MeOH) λ_{max} (log ε) 215 (3.92), 290 (375), 328 (3.59) nm; IR (KBr) ν_{max} 3368, 3046, 2964, 1684, 1660, 1618, 1536, 1473, 1359, 1264, 1139, 1064, 804 cm^{-1}; ^1H NMR and ^{13}C NMR data ($CDCl_3$, 500 and 125 MHz), see Table 1; positive ESIMS *m/z* 291 $[M + Na]^+$; positive HRESIMS *m/z* 291.1114 $[M + Na]^+$ (calcd for $C_{16}H_{16}N_2NaO_2$, 291.1109).

Asperfumigatone G (7) obtained as a pale yellow gum; UV (MeOH)

Table 1
^1H and ^{13}C NMR data for compounds **1**–**3** (in $CDCl_3$, 125 and 500 MHz).

No.	Compound **1**		Compound **2**		Compound **3**	
	δ_C, type	δ_H (m, *J*, Hz)	δ_C, type	δ_H (m, *J*, Hz)	δ_C, type	δ_H (m, *J*, Hz)
2	121.9, CH	6.93 s	124.3, CH	6.53 s	121.6, CH	6.92 s
3	112.2, C		112.8, C		111.9, C	
4	122.7, CH	6.86 s	122.5, CH	7.43 s	113.5, CH	6.62 s
5	115.7, C		115.4, C		116.9, C	
6	153.8, C		154.0, C		146.3, C	
7	98.8, CH	6.54 s	98.8, CH	6.45 s	140.6, C	
8	138.6, C		138.1, C		130.6, C	
9	118.9, C		119.8, C		118.0, C	
10	48.1, CH_2	3.63 s	47.9, CH_2	3.62 s	47.7, CH_2	3.62 s
11	203.6, C		203.5, C		203.3, C	
12	30.2, CH_3	2.15 s	30.3, CH_3	2.14 s	30.3, CH_3	2.16 s
13	118.1, CH	6.66 d (9.8)	118.0, CH	6.66 d (9.8)	118.7, CH	6.66 d (9.8)
14	128.4, CH	5.83 d (9.8)	128.6, CH	5.82 d (9.8)	128.7, CH	5.84 d (9.8)
15	80.1, C		80.2, C		80.4, C	
16	28.2, CH_3	1.55 s	28.2, CH_3	1.57 s	28.3, CH_3	1.54 s
17	28.2, CH_3	1.55 s	28.2, CH_3	1.57 s	28.3, CH_3	1.54 s
1-CH_3			33.6, CH_3	3.51 s		
NH		8.29 s				8.25 s
7-OCH_3					61.0, CH_3	3.83 s

λ_{max} (log ε) 215 (3.98), 293 (3.79), 330 (3.62) nm; IR (KBr) ν_{max} 3370, 3056, 2968, 1682, 1662, 1621, 1543, 1482, 1352, 1269, 1157, 1072, 829 cm^{-1}; ^1H NMR and ^{13}C NMR data ($CDCl_3$, 500 and 125 MHz), see Table 1; positive ESIMS *m/z* 321 $[M + Na]^+$; positive HRESIMS *m/z* 321.1224 $[M + Na]^+$ (calcd for $C_{17}H_{18}N_2NaO_3$, 321.1215).

2.5. Anti-G. Cichoracearum activity assays

The fungus *G. cichoracearum* was isolated from a tobacco plant exhibiting disease symptoms in a greenhouse located in Kunming, P. R. China. Dr. W.L. Yang from the Yunnan Academy of Tobacco Agricultural Sciences conducted the morphological identification of the fungus. The fungi were cultivated using *N. tabacum* cv. HD, a commonly cultivated tobacco variety in China, as the host plant in a sterile seedling environment. Moreover, a batch of sterile seedlings were separately cultivated, and 4–5 fully developed tobacco plants with true leaves were employed for the antifungal test.

2.5.1. Investigation of inhibition rate against G. Cichoracearum

The propagated fungi were collected from tobacco leaves in an ultra-clean workbench and diluted in 0.1% Tween-20 aqueous solution to a concentration of 1×10^5 conidia/mL of pathogen conidial suspension. This pathogen solution was then sprayed onto 4–5 true leaves-stage sterile tobacco seedlings, and each plant received 1.0 mL of spray. After 6 h, 1.0 mL of the test compound (250 μg/mL, dissolved in a 0.1% Tween-20 aqueous solution) was evenly applied to the tobacco leaves with a fine brush. The tissue culture bottle cap was then resealed, and the tobacco was cultured under a tissue culture lamp. After 7 days, the tobacco seedlings were processed, and leaves of similar size and growth were selected for assessing the infected area. A 0.1% aqueous solution of Tween-20 was used as the negative control, while carbendazim ($C_9H_9N_3O_2$, CAS No. 10605–21-7), a commonly used commercial antifungal pesticide for powdery mildew diseases in China, was utilized as the positive control. The inhibition rates were calculated using the following formula:

$$\text{inhibition rate } (\%) = [(C - T)/C] \times 100\% \quad (1)$$

where C is the (average infected spots area)/(total leaf area) of negative control, T is the (infected spots area of the treatment)/(total leaf area). All results are presented as the mean of three parallel treatments.

2.5.2. Investigation of protection activities against G. Cichoracearum

For the protective effects assay, sterile tobacco seedlings were planted by potting, and 250 μg/mL of the tested compounds and carbendazim (dissolved in 0.1% of Tween-20 aqueous, 1.0 mL) were evenly smeared on the whole leaves of 4–5 true leaves-stage tobacco plants as the treatment, and 0.1% of Tween-20 aqueous solution was used as the negative control. After 24 h, 1.0 mL of the pathogen solutions (1×10^5 conidia/mL) were sprayed onto the whole leaves of the pre-treated tobacco plants. After 7 days, the tobacco seedlings were selected to count the infected spots area. The inhibition rate was calculated by formula I. All results are expressed as the average of three parallel treatments.

2.5.3. Investigation of curative activities against G. Cichoracearum

In curative effects assay, sterile tobacco seedlings were planted by potting. The tobaccos with similar levels of powdery mildew infection were selected for the experiment. 1.0 mL of the test compound at a concentration of 250 μg/mL (dissolved in a 0.1% Tween-20 aqueous solution) was evenly applied to the entire leaf surface of tobacco plants, with a 0.1% Tween-20 aqueous solution used as a negative control. The remissions of the disease were observed on days 1, 3, 5, and 7, and the efficacy was recorded by taking pictures.

2.6. Spore observation

The pretreatment process for the tobacco plants followed the same steps as described for the curative effects assay in section 2.5.3. The conidiospores of *G. cichoracearum* were observed on day 7. The conidiospores of *G. cichoracearum* were carefully collected from the surfaces of leaves using transparent tape. Subsequently, these conidiospores were carefully placed onto microscope slides for further examination and observation. Examination and photography of the slides were conducted using a fluorescence biological microscope (Olympus CX33, Tokyo, Japan) at 100× lmagnification (10 × 10).

2.7. Paraffin section

The pretreatment process for tobacco plants was identical to that described in section 2.5.3. The paraffin sections of leaves were observed on day 7. Permanent slices of leaves from various treatments were prepared using the paraffin sectioning method. Briefly, leaves were cut into 2 mm × 3 mm samples and fixed in FAA fixation solution (95% ethanol, purified water, formaldehyde, glacial acetic acid, V/V/V/V = 10,7:2:1). The samples were then dehydrated using a 75%–100% ethanol gradient, cleared with xylene, impregnated with wax, embedded, sectioned, dewaxed, and stained with safranin and fast green staining solutions to make permanent sections. For sectioning, a semi-automatic rotary microtome (Leica RM2255, Europe) was used to achieve a thickness of 8 μm. Microscopic examination was conducted using a fluorescence biological microscope (Olympus CX33, Tokyo, Japan) at 200× magnification (10 × 20).

2.8. Defense enzyme activities assay

The enzymatic activities of phenylalanine ammonia lyase (PAL), peroxidase (POD), polyphenol oxidase (PPO), superoxide dismutase (SOD), catalase (CAT), and ascorbate peroxidase (APX) were assessed using assay reagent kits (Jiancheng Bioengineering Research Institute, Nanjing, P.R. China), following the manufacturer's instructions. The protocols used in the study also refer to the previous description (Hu et al., 2022). The host plants used in this experiment were *N. tabacum* cv. HD plants. Spray 1.0 mL of a spore suspension with a concentration of 1×10^5 conidia/mL onto sterile seedlings. Following a 24 h infection period with *G. cichoracearum*, the tobacco leaves were treated with a spray solution containing 250 μg/mL of the tested compounds (1.0 mL). Healthy tobacco was denoted as mock, treated with *G. cichoracearum* in a 0.1% Tween-20 aqueous solution as the negative control (T + G), treated with carbendazim as the positive control (C + G), with groups **7** (**7** + G) and **9** (**9** + G) serving as the treatment groups. The leaves were then collected on days 1, 3, 5, and 7, and the activities of the aforementioned enzymes were measured.

2.9. Analysis of SA, JA, MDA, and CHL content

The levels of salicylic acid (SA), jasmonic acid (JA), malondialdehyde (MDA), and chlorophyll (CHL) were measured using assay reagent kits for SA, JA, MDA, and CHL (Comin Bioengineering Institute, Suzhou, P.R. China), following the manufacturer's instructions. The pre-treatment process was the same as described in 2.8. Subsequently, the contents of SA, JA, MDA and CHL in leaves on days 1, 3, 5 and 7 were evaluated. The CHL contents were quantified as the sum of chlorophyll-a and chlorophyll-b.

2.10. Quantitative real-time PCR analysis of defense-related genes

Quantitative real-time PCR (qRT-PCR) analysis of defense related genes (*PR-1*, *PR-5*, *PAL* and *Chit-1*) in this part was carried out according to the reported methods (Yan et al., 2022). The pre-treatment process was the same as described in 2.8. To perform qRT-PCR analysis of

defense-related genes, total RNA was extracted from 0.3 g of tobacco leaves (fresh weight) using the RNA Easy kit from TianGen Biotech Co., Ltd., Beijing, P.R. China, following the instructions provided by the manufacturer. The purified RNA was subjected to reverse transcription using oligo (dT) primers and SuperScript III Reverse Transcriptase (Invitrogen) according to the manufacturer's instructions. To quantify the expression levels of *PR-1*, *PR-5*, *PAL*, and *Chit-1*, qRT-PCR was conducted using the TaKaRa SYBR Premix Ex Taq kit on the ABI PRISM 7500 system (Applied Biosystems).

2.11. Molecular docking

Tubulin from *G. cichoracearum* was used as the target for molecular docking calculations using AutoDock Vina software. The protein sequence was obtained from the NCBI database (GenBank: RKF84170.1) following the previously described method (Sachse et al., 2007). The construction of the 3D protein structures utilized homology modeling with Modeller 10.1, while Chem3D was employed for the generation of the ligand structures. To facilitate molecular docking calculations, the proteins and ligands were prepared in accordance with the AutoDock protocol, resulting in the generation of pdbqt files. The docking grid, sized 40 Å * 40 Å * 40 Å, was designated as the receptor binding site. The grid spacing values were modified to 0.375 Å, and Gasteiger atomic partial charges were allocated to all ligands under investigation.

3. Results and discussion

3.1. Structure elucidation

In our continuous exploration of the microorganisms derived from *N. tabacum*, the EtOAc extract acquired from the fermentation of *A. fumigatus* 0338 was fractionated by repeated CC including silica gel and semi-preparative HPLC to yield seven undescribed indole alkaloid derivatives (**1**–**7**) along with seven previously known analogs (**8**–**14**). The structures of these compounds are displayed in Fig. 1, the ^{1}H and ^{13}C NMR data for novel compounds are listed in Tables 1–3. Comparison of the ^{1}H and ^{13}C NMR data with those previous literature, the known isolates were ascertained as 1-(6-methoxy-5-prenyl-1*H*-indol-3-yl)-propan-2-one (**8**) (Ma et al., 2023), 9-methoxyolivacine (**9**) (Schmidt et al., 2018), psammocindoles B (**10**) (Kwon et al., 2021), dilemmaone B (**11**) (Beukes et al., 1998), 3-acetonylidene-7-prenylindolin-2-one (**12**) (Zhang et al., 2014), 3-prenyl-5-(3-keto-but-1-enyl)-indole (**13**) (Fujimoto et al., 2021) and bruceolline H (**14**) (Chen et al., 2011).

Compound **1** was isolated as a pale yellow gum, and its molecular formula was established as $C_{16}H_{17}NO_2$ by positive HRESIMS, implying an index of hydrogen deficiency of nine. The IR spectrum displayed peaks at 3379 cm^{-1} (amino group), 1684 cm^{-1} (carbonyl), and 1620, 1558, 1482 cm^{-1} (aromatic ring). Detailed analysis of the 1D NMR, DEPT and HSQC spectra, revealed the presence of a carbonyl carbon, an oxygenated sp^3 quaternary carbon, five nonprotonated aromatic carbons, five methines, a methylene and three methyls carbon. The HMBC correlations (Fig. 2) of H-2 (δ_H 6.93, s) with C-3/C-8/C-9, H-4 (δ_H 6.86, s) with C-3/C-5/C-6/C-8/C-9/C-13, H-7 (δ_H 6.54, s) with C-5/C-6/C-8/C-9, H-13 (δ_H 6.66, d, J = 9.8 Hz) with C-4/C-5/C-6/C-14/C-15, H-14 (δ_H 5.82, d, J = 9.8 Hz) with C-5/C-13/C-15, NH (δ_H 8.29, s) with C-2/C-3/C-8/C-9 allowed the elucidation of the basic structure of **1**, similar to previously described compounds (Li et al., 2019). Since the indole skeleton was determined, the positions of remaining substituents also can be determined by further analysis of its HMBC data (Fig. 2). The existence of 2-oxopropyl part was clearly indicated by the HMBC correlations of H_2-10 (δ_H 3.63, s) with C-11/C-12, and H_3-12 (δ_H 2.15, s) with C-10/C-11 and this part located to C-3 due to the HMBC correlations of H_2–10 with C-2/C-3/C-9. Further HMBC correlations of H_3-16 and H_3-17 with C-14/C-15 supported the attachment of these two methyls to C-15. Thus, compound **1** was clarified as shown and named asperfumigatone A.

Asperfumigatones B and C (compounds **2** and **3**) were acquired as pale yellow gum. The molecular formulas of **2** and **3** were found to be $C_{17}H_{19}NO_2$ and $C_{17}H_{19}NO_3$ by HRESIMS, respectively. Compounds **1**–**3** have an identical index of hydrogen deficiency, similar UV, IR, and NMR data suggested that above compounds are analogues. Detailed analysis of the NMR spectroscopic data (Table 1) revealed that **2** has nearly the same structure as **1**, differing only by the replacement of the hydrogen at N-1 with a methyl (δ_H 3.51, s; δ_C 33.6). This observation was deduced from the HMBC correlations (Fig. 2) of H_3-1-CH_3 with C-2/C-8. The deshielded resonance of C-7 (δ_C 140.6) suggested that it was oxygenated, and the HMBC correlations of H_3-7-OCH_3 with C-7, supported methoxy substitution (δ_H 3.83, s; δ_C 61.0) at C-7 in **3**. Thus, the structures of asperfumigatones B and C were determined as shown.

Table 2
^{1}H and ^{13}C NMR data for compounds **4**–**5** (in $CDCl_3$, 125 and 500 MHz).

No.	Compound **4**		Compound **5**	
	δ_C, type	δ_H (m, *J*, Hz)	δ_C, type	δ_H (m, *J*, Hz)
2	121.3, CH	6.80 s	124.7, CH	6.58 s
3	116.2, C		116.8, C	
4	121.2, CH	6.90 s	121.3, CH	7.14 s
5	119.8, C		119.6, C	
6	151.3, C		151.2, C	
7	100.7, CH	6.55 s	100.4, CH	6.42 s
8	136.9, C		135.4, C	
9	120.2, C		120.9, C	
10	48.2, CH_2	3.66 s	48.1, CH_2	3.66 s
11	203.3, C		203.5, C	
12	30.5, CH_3	2.13 s	30.3, CH_3	2.15 s
13	26.9, CH_2	3.29 d (7.6)	27.1, CH_2	3.31 d (7.6)
14	123.7, CH	5.42 t (7.6)	123.7, CH	5.42 t
15	132.6, C		132.9, C	
16	17.7, CH_3	1.78 s	17.6, CH_3	1.79 s
17	25.8, CH_3	1.88 s	25.7, CH_3	1.89 s
NH		8.23, br s		
6-OH		10.27, br s		10.24, br s
1-CH_3			33.9, CH_3	3.54 s

Table 3
^{1}H and ^{13}C NMR data for compounds **6**–**7** (in $CDCl_3$, 125 and 500 MHz).

No.	Compound **6**		Compound **7**	
	δ_C, type	δ_H (m, *J*, Hz)	δ_C, type	δ_H (m, *J*, Hz)
2	121.9, CH	6.83 s	121.2, CH	6.84 s
3	116.2, C		116.3, C	
4	119.2, CH	7.48 s	112.5, CH	7.14 s
5	123.7, C		126.9, C	
6	124.9, C		110.6, C	
7	112.5, CH	6.96 s	144.9, C	
8	140.1, C		132.6, C	
9	125.3, C		128.6, C	
10	48.4, CH_2	3.64 s	48.1, C	3.63 s
11	203.5, C		203.3, CH_3	
12	30.6, CH_3	2.13 s	30.5, CH_3	2.14 s
13	168.5, C		168.2, C	
14	131.8, CH	6.45 s	131.3, CH	6.45 s
15	133.6, C		133.8, C	
16	53.8, CH_2	4.55 d (5.4)	53.6, CH_2	4.55 d (5.4)
17	19.8, CH_3	1.82 s	19.7, CH_3	1.83 s
NH		8.47 s		8.45 br s
NH		5.61 t (5.4)		5.60 t
-OCH_3			60.2	3.85 s

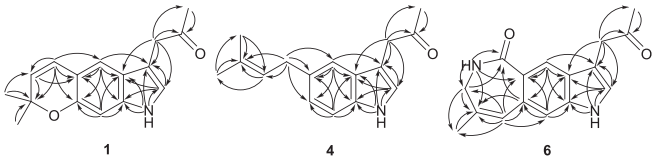

Fig. 2. Key HMBC correlations of compounds **1**, **4** and **6**.

Asperfumigatone D (**4**), isolated as a pale yellow gum, had a molecular formula of $C_{16}H_{19}NO_2$ obtained by HRESIMS spectrum, reflecting nine degrees of unsaturation. The ^1H, ^{13}C NMR, DEPT and HSQC spectra indicated the presence of three methyl groups CH_3-12 (δ_H 2.13, s; δ_C 30.5), CH_3-16 (δ_H 1.78, s; δ_C 17.7) and CH_3-17 (δ_H 1.88, s; δ_C 25.8), two methylene groups CH_2-10 (δ_H 3.66, s; δ_C 48.2) and CH_2-13 (δ_H 3.29, d, $J = 7.6$ Hz; δ_C 26.9), four aromatic methine groups CH-2 (δ_H 6.80, s; δ_C 121.3), CH-4 (δ_H 6.90, s; δ_C 121.1), CH-7 (δ_H 6.55, s; δ_C 100.7) and CH-14 (δ_H 5.42, t, $J = 7.6$ Hz; δ_C 123.7), six aromatic quaternary carbons C-3/5/6/8/9/15 (δ_C 116.8/119.8/151.3/136.9/120.2/132.6), a carbonyl carbon C-11 (δ_C 203.3) and two exchangeable protons 1-NH (δ_H 8.23, br s) and 6-OH (δ_H 10.27, br s) (Table 2). The HMBC correlations of NH with C-2/C-3/C-8/C-9, H-2 with C-3/C-8/C-9/C-10, H-4 with C-3/C-5/C-6/C-8/C-9, H-7 with C-5/C-6/C-8/C-9, H_2-10 with C-2/C-3/C-9/C-11/C-12, H_3-12 with C-10/C-11 (Fig. 2) indicated that the presence of a 3-oxopropyl-5,6-trisubstituted-indole skeleton in compound **4**. In addition, the HMBC correlations (Fig. 2) of H_2-13 with C-4/C-5/C-6/C-14/C-15, H-14 with C-5/C-13/C-15/C-16/C-17, H_3-16 with C-14/C-15/C-17 and H_3-17 with C-14/C-15/C-16 supported that there is a prenyl group at C-5. The hydroxyl substituent at C-6 were deduced through the HMBC correlations of active proton at δ_H 10.27 with C-5/C-6/C-7. Taken together, the structure of **4** was confirmed and its structural features were highly similar to those of previously described (Ma et al., 2023).

Asperfumigatone E (**5**) was isolated as a pale yellow gum, providing a molecular formula of $C_{17}H_{21}NO_2$, with a molecular mass 14 Da more than that of **4**, same degrees of unsaturation as **4**. And the UV, IR and NMR spectra of **5** were highly similar to those of **4**. Comparison of the ^1H and ^{13}C NMR spectra between **4** and **5** revealed that the amino proton in **4** was substituted by a methyl group (δ_H 3.54, s; δ_C 33.9) in **5** (Table 2). This was confirmed by the HMBC correlations of H_3-1-CH_3 with C-2/C-8 (Fig. 2). Ultimately, compound **5** was identified.

Asperfumigatone F (**6**) was purified as a pale yellow gum, with a molecular formula of $C_{16}H_{16}N_2O$, indicating 10 degrees of unsaturation. Detailed analysis of its ^1H NMR, ^{13}C NMR, DEPT, and HSQC spectra revealed the presence of two methyl groups, two methylene groups, four methine groups, eight aromatic quaternary carbons (including a carbonyl carbon and one amide carbon), as well as two active protons. The HMBC correlations of NH (δ_H 8.47, br s) with C-2/C-3/C-8/C-9, H-2 (δ_H 6.83, s) with C-3/C-8/C-9/C-10, H-4 (δ_H 7.48, s) with C-3/C-5/C-6/C-8/C-9, H-7 (δ_H 6.96, s) with C-5/C-6/C-8/C-9, H_2-10 (δ_H 3.64, s) with C-2/C-3/C-9/C-11/C-12, and H_3-12 (δ_H 2.13, s) with C-10/C-11 (Fig. 2), indicated that the presence of a 3-oxopropyl-5,6-trisubstituted indole moiety within compound **6** same as **4**. Accounting for three remaining degrees of unsaturation, except for one carbonyl and two olefinic carbons, implied the existence of an additional ring in the structure. Further HMBC correlations of NH (δ_H 5.61, s) with C-5/C-13/C-15/C-16, H-14 (δ_H 6.45, s) with C-5/C-6/C-7/C-15/C-16/C-17, H_2-16 (δ_H 4.55, d, $J =$ 5.4 Hz) with C-13/C-14/C-15/C-17, H_3-17 (δ_H 1.82, s) with C-14/C-15/C-16, H-4 with C-13 and H-7 with C-14 indicated the presence of a methyl-substituted lactam seven-member ring fused to positions C-5 and C-6 of the indole ring as depicted in Fig. 2. Thus, compound **6** was established.

Compound **7**, a pale yellow gum, has a molecular formula of $C_{17}H_{18}N_2O_3$ and the same number of degrees of unsaturation as **6**. The NMR spectra of the two compounds are highly similar (Table 3), with the exception of lacking an aromatic proton δ_H 6.96 (s) in **6**, and exhibiting a methoxy signal δ_H 3.85 (s), δ_C 60.2 in **7**. This can be inferred from the HMBC correlation of the methoxy hydrogen at δ_H 3.85 with C-7 (Fig. 2) and downfield shift of the chemical shift at C-7 from 112.5 to 144.9. Therefore, the structure of **7** was determined and named asperfumigatone G.

3.2. Determination of inhibition, protection, and curative activities of compounds 1–14

Considering that indole alkaloids have significant inhibitory effects on fungi (Liu et al., 2020b) and that the fungus *G. cichoracearum* is the main pathogen of tobacco powdery mildew (Guo et al., 2023; Liu et al., 2016), we evaluated the efficacy of compounds **1**–**14** on *G. cichoracearum*. The antifungal activity was tested according to method described in previous studies (Quaglia et al., 2012; Wang et al., 2012a). The results revealed that compounds **7** and **9** demonstrated obvious anti-*G. cichoracearum* activities with an inhibition rate of 82.6% ± 5.6 and 85.2% ± 5.7, respectively. As shown in Table 4, the inhibition rates of compounds **7** and **9** against *G. cichoracearum* were higher than that of carbendazim (78.6% ± 6.1). Moreover, compared to the negative control (Fig. S21), compounds **1**–**14** exhibited significant antifungal activities against *G. cichoracearum*, with inhibition rates ranging from 35.7% ± 5.6 to 85.2% ± 5.7.

Considering those compounds **6**, **7**, **9**, **12** and **14** had significant inhibitory rates above 60%, the protective effects of these compounds against *G. cichoracearum* were also evaluated. According to the data presented in Table 5 and Fig. S22, compound **9** (250 μg/mL) exhibited a superior protective effect with an inhibition rate of 85.4% ± 6.0, which was stronger than that of carbendazim (82.3% ± 6.2) at the same concentration. The protective effect of compound **7** was comparable to carbendazim, with inhibition rate of 82.2% ± 6.4. In comparison to the negative control, compounds **6**, **12**, and **14** exhibited notable effects on *N. tabacum* cv. HD plants infected with *G. cichoracearum* (Fig. S22). These findings indicate that preconditioning host plants with compounds **7** and **9** can significantly enhance their resistance to *G. cichoracearum* infection.

From these results, compounds **7** and **9** had the strongest inhibition rates and protective effects on *G. cichoracearum*, and their curative effects were also tested on *N. tabacum* cv. HD. As depicted in the Fig. 3, the negative control group showed significant lesions and stunted leaf growth after *G. cichoracearum* infected. However, after treatment with compounds **7**, **9** and carbendazim (250 μg/mL), there was a noticeable reduction in the number of lesions, and the leaves grew more normally, exhibiting significantly better vigor than the negative control group. Upon close examination of the leaf surface, the number of lesions decreased sequentially for compounds **7**, **9**, and carbendazim during the same period. These research findings indicate that compounds **7** and **9** have effective therapeutic action against powdery mildew, with **9** being superior, exceeding the positive control's performance.

3.3. Observation of spores on leaf surface

Based on the previous studies, compound **9** exhibited the highest level of activity, suggesting its significant role in inhibition and curative effects, as well as its potential to induce plant resistances. Therefore, we conducted microscopic observations of *G. cichoracearum* on the leaf surface. The result showed that within 24 h of being sprayed with 250 μg/mL of compound **9** (Fig. 4b), the majority of the conidiospores exhibited significant shrinkage, and the internal structures of the spores

Table 4
Inhibitory effects of compounds **1**–**14** on *G. cichoracearum* in tobacco leaves (250 μg/mL).

No.	Inhibition rates (%)	No.	Inhibition rates (%)
1	48.2 ± 6.0^{efg}	**9**	85.2 ± 5.7^{a}
2	35.7 ± 5.6^{h}	**10**	52.6 ± 5.9^{defg}
3	53.6 ± 6.2^{defg}	**11**	49.4 ± 6.0^{defg}
4	42.8 ± 5.8^{gh}	**12**	60.2 ± 5.7^{bcd}
5	46.5 ± 5.2^{fg}	**13**	55.4 ± 5.5^{cdef}
6	68.4 ± 6.0^{b}	**14**	65.4 ± 5.2^{bc}
7	82.6 ± 5.6^{a}	carbendazim	78.6 ± 6.1^{a}
8	58.9 ± 6.0^{bcde}		

Note: Different lowercase letters in the same column indicate significant differences among various compounds at the 0.05 level, as determined by Duncan's multiple range test. The means ± standard deviations (SDs) of the data were obtained from three replicates and are presented.

Table 5
Protective effects of compounds **6**, **7**, **9**, **12** and **14** against *G. cichoracearum* on tobacco leaves (250 μg/mL).

No.	Protective effects (%)
6	68.8 ± 5.6^{b}
7	82.2 ± 6.4^{a}
9	85.4 ± 6.0^{a}
12	56.8 ± 6.0^{c}
14	60.2 ± 5.6^{bc}
carbendazim	82.3 ± 6.2^{a}

Note: Different lowercase letters in the same column indicate significant differences among various compounds at the 0.05 level, as determined by Duncan's multiple range test. The means ± standard deviations (SDs) of the data were obtained from three replicates and are presented.

were noticeably distorted. By day 7 (Fig. 4c), the conidiospores had undergone further shrinkage and deformation, making normal spores almost indiscernible. These observations suggest that compound **9** can directly target and affect the conidiospores of *G. cichoracearum*.

3.4. Observation of leaf transverse section

To assess the impact of compound **9** on the tissue structure of tobacco leaves infected with *G. cichoracearum*, we employed paraffin sectioning techniques. This technique allowed us to observe any changes occurring in the tissue structure following the application of compound **9** (250 μg/mL). In healthy tobacco leaves, prior to inoculation with *G. cichoracearum*, the cells were plump and closely arranged, with clear boundaries delineating the tissue structure. Within the leaf, two types of mesophyll cells were present: elongated palisade histiocytes and ovoid spongy histiocytes, each with distinctive structural characteristics (Fig. 5a). Typically arranged in one or two layers, the palisade cells formed a neat fence-like pattern on the adaxial surface of the leaves, with minimal intercellular gaps. However, on day 7 after infection without treatment with **9**, the palisade cells displayed deformations, accompanied by an increase in intercellular space. Furthermore, the distinct boundary between the palisade cells and the spongy tissue became less clear. As the pathogenic hyphae continued to spread, the structure of the palisade cells transformed from oblong-shaped cells to multiple elongated and twisted cells (Fig. 5b). In contrast, on day 7 after

Fig. 3. Curative effects of compounds **7**, **9**, and carbendazim (250 μg/mL) on infected *N. tabacum* cv. HD on days 3 (up) and 7 (down). **a** and **e**, treatment with 0.1% Tween-20 aqueous solution (negative control); **b** and **f**, treatment with compound **7**; **c** and **g**, treatment with compound **9**; **d** and **h**, treatment with carbendazim.

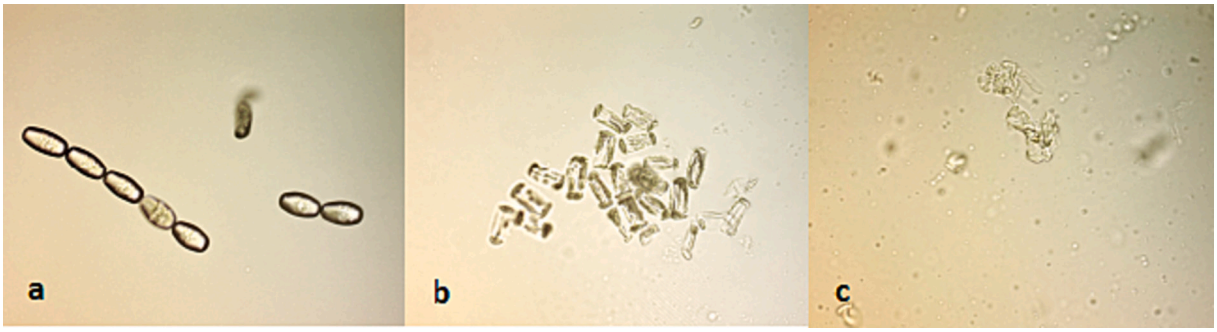

Fig. 4. Effects of compound **9** (250 μg/mL) on the conidiospores of *G. cichoracearum* observed under a microscope. **a**–**c**: 100×; **a**: treatment with 0.1% Tween-20 aqueous solution (negative control); **b**: treatment with **9** on day 1; **c**: treatment with **9** on day 7.

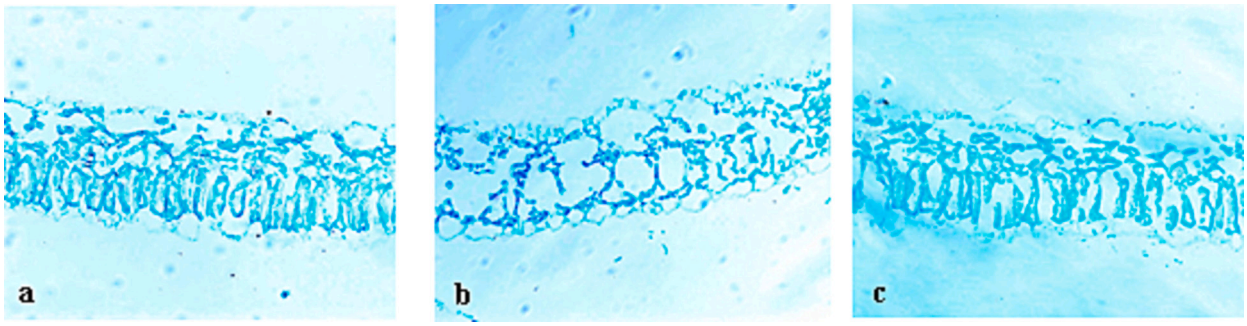

Fig. 5. Changes in tissue structure of infected *N. tabacum* cv. HD leaves after treatment with compound **9** (250 μg/mL). **a**–**c**: 200×; **a**: healthy tobacco; **b**: on day 7 without treatment with **9**; **c**: on day 7 treatment with **9**.

treatment with 250 μg/mL of **9** (Fig. 5c), the tissue structure of the leaves appeared more compact, and the overall tissue morphology began to gradually resemble that of healthy leaves once again. The palisade tissue exhibited a neat and tight arrangement, while the spongy tissue was close to the palisade tissue, with a clear structural boundary. Notably, the thickness and regular arrangement of both the palisade and spongy tissues significantly increased after treatment with **9**. This enhancement in tissue characteristics contributes to a strengthened resistance against the pathogens.

3.5. Effects of compounds *7* and *9* on defense-related enzyme activities

Considering the significant correlation between activities of defense enzymes and plant resistance (Dietz et al., 2016; Liu et al., 2020a), we analyzed the activities of six enzymes in tobacco leaves treated with compounds **7** and **9**. As shown in Fig. 6, enzyme activities of the mock group were lower than those observed in the T + G, C + G, **7** + G, and **9** + G groups. It is worth noting that after treatment with compounds **7** or **9**, the changes of PAL, CAT and APX were more pronounced, while the changes of SOD, POD and PPO were not obvious. In Fig. 6b, the PAL activities in the **7** + G and **9** + G groups on day 3 were the highest. Specifically, PAL activity in the **7** + G group was 2.62-fold higher than the mock, 2.0-fold higher than the T + G, and 1.74-fold higher than the C + G. The **9** + G group was 2.77-fold higher than the mock, 2.11-fold higher than the T + G, and 1.85-fold higher than the C + G. PAL is involved in the phenylpropanoid metabolism pathway, converting phenylpropanoids into cinnamic acid and producing SA to defend against pathogens. Thus, an increase in PAL enzyme activity may enhance plant resistance (Dietz et al., 2016; Liu et al., 2020a). Interestingly, the activity of CAT also reached its maximum on day 3 after treatment. The activity of CAT significantly increased after tobacco plants were infected with fungi. However, a significant decrease in CAT activity was observed in Fig. 6e when compared to the T + G group. CAT is widely present in plants and can eliminate H_2O_2, which is toxic to plants during metabolic processes. These findings indicate the importance of a significant decrease in CAT activity to maintain a balanced concentration of ROS, thereby improving resistance when tobacco is infected with powdery mildew. In Fig. 6f, a noticeable increase in APX activity was observed from day 1 to day 5 in both the **7** + G and **9** + G groups. The **7** + G group was 1.40 times higher than the T + G group and the **9** + G group was 1.45 times higher. APX is critical in clearing H_2O_2 in plants, especially within chloroplasts. Under stress, APX can rapidly remove excess hydrogen peroxide from cells, reducing the damage from ROS to plant cells (Yan et al., 2016). Therefore, an increase in APX enzyme activity may enhance plant resistance. In addition, the expression of PPO was enhanced in the C + G, **7** + G, and **9** + G groups on day 7. PPO can create a protective film by catalyzing the synthesis of lignin and quinone components, protect cells from pathogens, and play a direct role in disease resistance (Zhao et al., 2017). The above defense enzymes such as PAL, CAT, APX and PPO play an important role in plant disease resistance. The activity of these defense enzymes directly affects the strength of plant disease resistance.

3.6. Effects of compounds *7* and *9* on plant signaling element content

JA and SA are key signaling molecules associated with plant resistance (Amil-Ruiz et al., 2016; Yang et al., 2018). Because PAL can induce SA and JA in tobacco plants, the contents of SA and JA were determined. SA is known to activate the SAR response in plants (Lim et al., 2016; Peng et al., 2021; Rienth et al., 2019). The results (Fig. 7a and Fig. 7b) revealed that after being treated with carbendazim, compounds **7** and **9** (250 μg/mL), the accumulation of SA and JA in tobacco plants increased. The change in SA content was more pronounced than in JA content. In the group treated with carbendazim and **7**, the SA content reached their highest level on day 5. In the group treated with **9**, the SA content peaked on day 3 and gradually decreased from day 3 to day 7. Notably, the changes in SA content in the **7** + G and **9** + G treatment groups showed a more favorable trend compared to the carbendazim treatment group (C + G) (Fig. 7a). These findings indicate that compounds **7** and **9** can reduce the degree of plant damage caused by *G. cichoracearum* infection in tobacco leaves.

MDA is an important indicator that reflects the level and degree of cell membrane peroxidation, serving as a measure of the plant's stress tolerance (Möller et al., 2020). Plants treated with disease-resistant substances produce a protective effect by inhibiting the growth of MDA in the plants. Hence, the contents of MDA were analyzed. In Fig. 7c, the changes in the mock group were not significant, while the MDA content in the T + G group showed an increasing trend. Compared with the T + G group, the MDA content in the **7** + G and **9** + G groups was significantly reduced and showed superior results compared to the C + G group. Therefore, pre-treatment with compounds **7** and **9** (250 μg/mL) can significantly inhibit the increase of MDA content and enhance plant disease resistance.

Additionaly, chlorophyll (CHL) is a key factor in plant photosynthesis, providing energy for plant growth (Fujimoto et al., 2021; Kim et al., 2021). As shown in Fig. 7d, after inoculation with *G. cichoracearum* (the T + G group), the chlorophyll content of the plant gradually decreased from day 1 to day 7. However, after treatment with carbendazim, compounds **7** and **9** (250 μg/mL), the chlorophyll content gradually increased. These results indicate that treatment with carbendazim, compounds **7** and **9** can enhance plant's photosynthetic capacity and resistance, and compounds **7** and **9** were better than carbendazim.

3.7. Effects of compounds *7* and *9* on defense-related genes

In plants, fungus resistance is closely related to the expression of defense gene. *PAL* gene is closely linked to the phenylpropanoid metabolism pathway and powdery mildew resistance (Singh et al., 2019). *Chit-1* plays a crucial role in the plant defense system, producing chitinase to efficiently break down the chitin constituents in the cell walls of

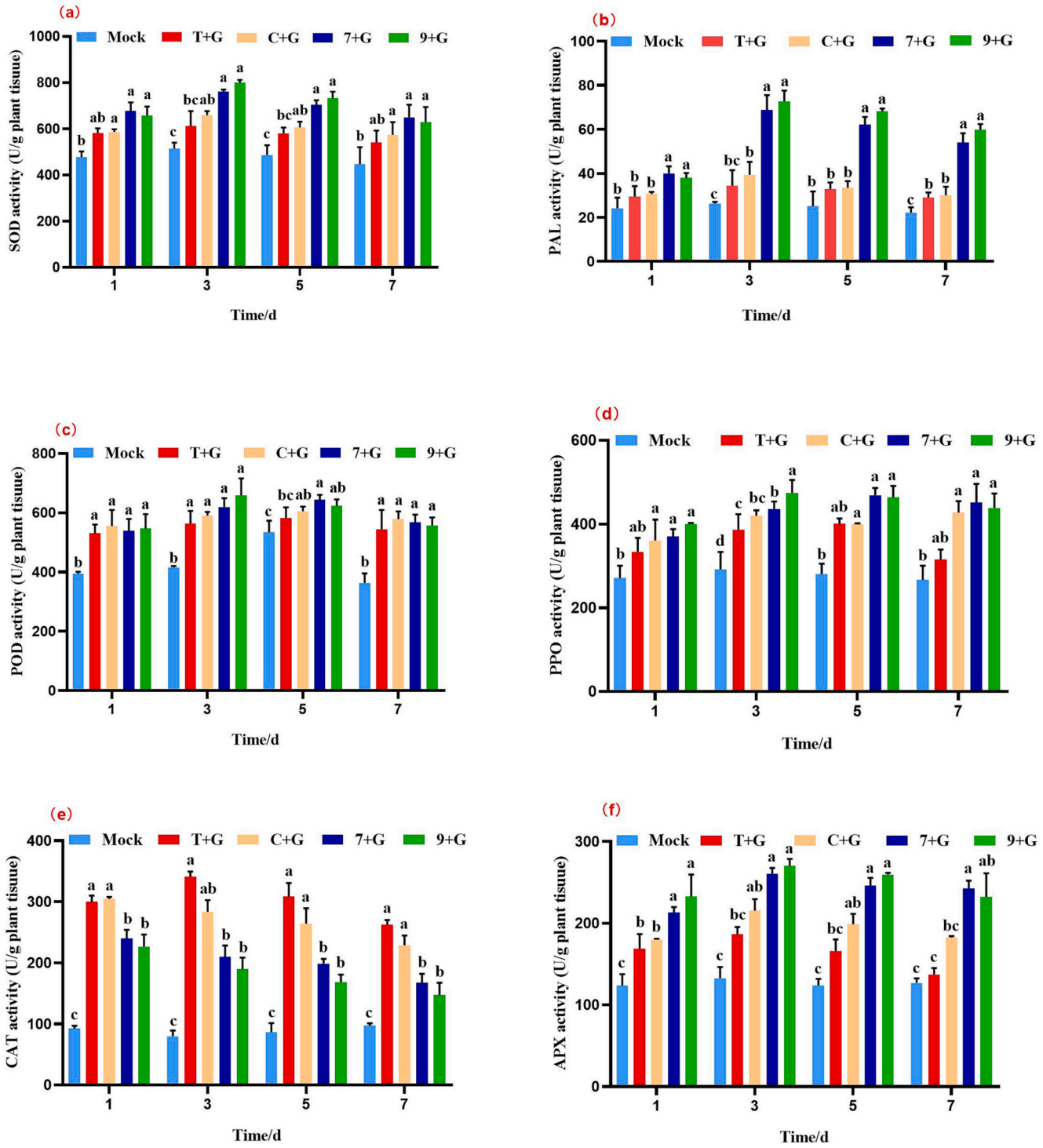

Fig. 6. Activities of SOD (**a**), PAL (**b**), POD (**c**), PPO (**d**), CAT (**e**) and APX (**f**) in tobacco leaves treated with 250 μg/mL of carbendazim, compounds **7** and **9**. Mock: healthy tobacco; T + G: *G. cichoracearum* in 0.1% of Tween-20 solution (negative control); C + G: treatment with carbendazim; **7** + G: treatment with **7**; **9** + G: treatment with **9**. All results were expressed as the average value of three measurements for all group.

higher fungi. This action effectively hampers and eliminates diverse plant pathogens (Dong et al., 2017). *PR-1* and *PR-5* are genes that serve as markers for SAR in plants. These two genes play a crucial role in pathogen defense by actively attacking pathogens, breaking down cell walls, and degrading pathogenic toxins (Guo et al., 2020a). Therefore, we analyzed the expression of the above genes in tobacco leaves (Fig. 8). In the mock and T + G groups, gene expression was relatively stable. In the C + G group, the expressions of *PAL* and *PR-1* were markedly up-regulated and reached the peak on day 5. However, after treatment with compounds **7** or **9**, the expression levels of *PAL*, *Chit-1*, *PR-1*, and *PR-5* were significantly upregulated. After treatment with **7**, the expression levels of *PAL* and *PR-1* reached their peak on day 5, while *Chit-1* and *PR-5* reached their peak on day 3. In the **9** + G group, the expression levels of *PAL*, *Chit-1*, *PR-1*, and *PR-5* were highest on day 3. This study demonstrates a strong correlation between fungus resistance and the upregulation of key defense genes in tobacco plants. Expression

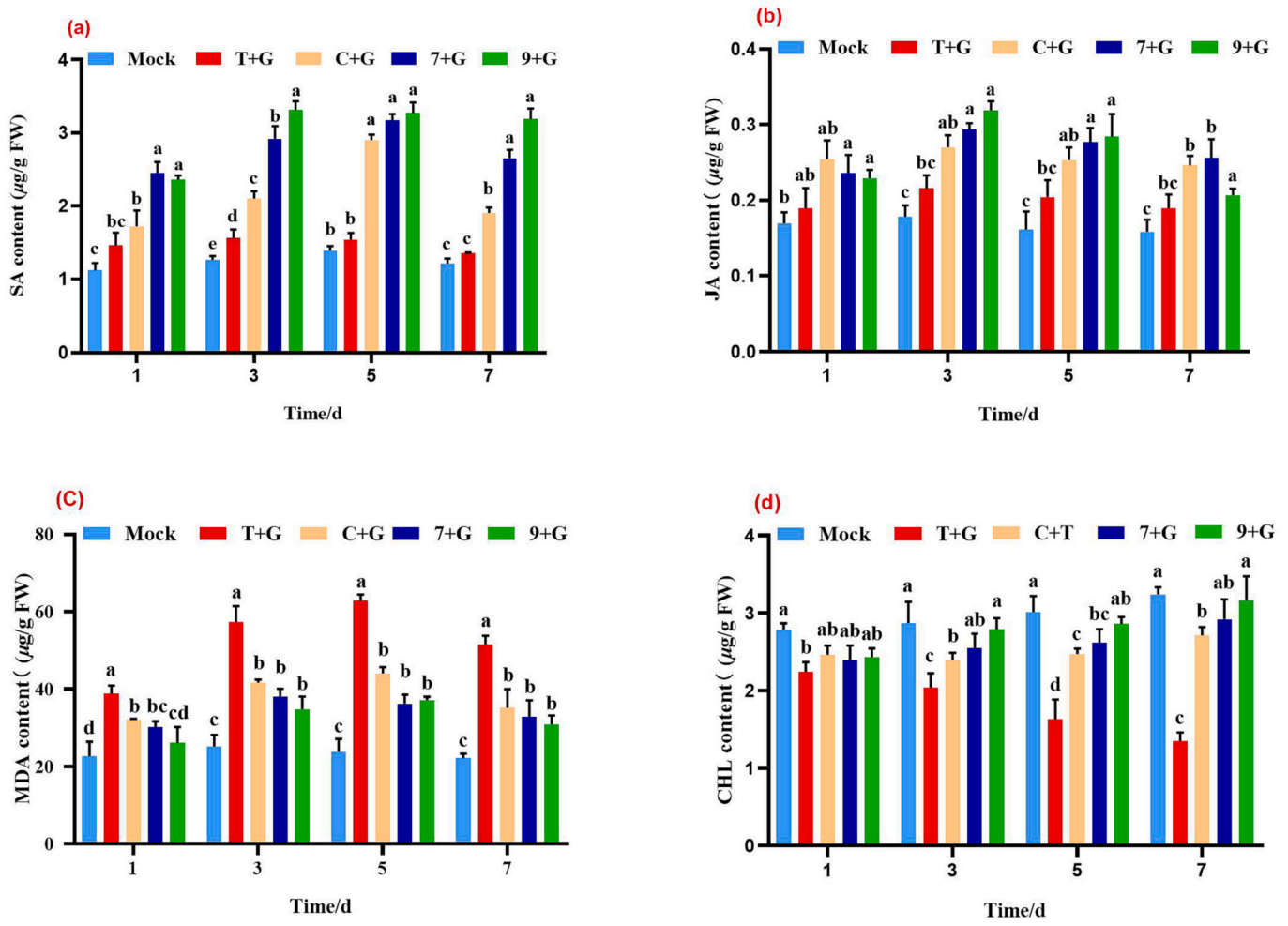

Fig. 7. Effects of 250 μg/mL of carbendazim, compounds **7** and **9** on the accumulation of SA (**a**), JA (**b**), MDA (**c**), and CHL (**d**) in tobacco leaves. Mock: healthy tobacco; T + G: *G. cichoracearum* in 0.1% of Tween-20 solution (negative control); C + G: treatment with carbendazim; **7** + G: treatment with **7**; **9** + G: treatment with **9**. All results were expressed as the average value of three measurements for all group.

of these genes was markedly increased upon treatment with antifungal compounds **7** and **9**, highlighting the compounds' effectiveness in triggering plant defense mechanisms against pathogenic fungi.

3.8. Molecular docking

Previous studies have demonstrated that the activity of fungicides against powdery mildew can be evaluated by the binding interaction between the compound and the tubulin of *G. cichoracearum* (Obydennov et al., 2021; Pathak et al., 2020). Molecular docking was conducted between compounds **1**–**14** and tubulin to further understand their binding modes. The docking analysis of **9** was depicted in Fig. 9 and the docking results of compounds **1**–**8** and **10**–**14** was displayed in Additional materials (Fig. S23). These compounds demonstrated strong interactions with the catalytic pocket of tubulin, which is essential for inhibiting *G. cichoracearum* activity. In terms of the structure-activity relationship, the indole parent nucleus in the structures of compounds **1**–**14** can form π–π stacking interactions with Phe257. In addition, the -NH- moiety of compound **1** forms a hydrogen bond with ILe240. The core structure of compound **2** lost this hydrogen bond, and consequently, its potency decreased. Compared to compound **1**, the interactions formed by compounds **3**–**5** are similar, but **3** is relatively rigid, which results in lower binding entropy and thus greater activity than that of compounds **4** and **5**. Furthermore, the interactions formed by compounds **6** and **7** are similar, but the presence of methoxy group in compound **7** enhances the hydrophobic interaction formed with Phe257, resulting in increased activity. The isopentenyl group in compound **8** may form hydrophobic bonds with Leu261 and Leu169, rendering it more active than compound **1**. Compound **9** forms additional π–π stacking interactions with Phe204 and Phe257, so the activity is the best. At the same time, compound 9 also showed the highest inhibition rate, protection effect and therapeutic effect in vivo antifungal experiments (Tables 4 and 5). Compounds **10** and **11** form hydrogen bonds with ILe240 and π–π stacking with Phe257, exhibiting activity similar to that of compound **1**. Compounds **12**–**14** were observed to form hydrogen bonds with ILe240 and engage in π–π stacking interactions with Phe257, and their side chains formed more hydrophobic interactions. These structural features suggest that compounds **12**–**14** might have enhanced activities compared to compound **1**. Docking results mentioned above were in agreement with the findings of the in vivo antifungal experiments (Tables 4 and 5). These results indicated that the indole nucleus has the capability to interact with tubulin protein. Additionally, in conjunction with the results of the activity tests (Tables 4 and 5), it seems that compounds with the parent structures of **6**, **7**, and **9** exhibit substantial *anti-G. cichoracearum* activity. Specifically, the presence of a methoxy substitute in compound **7** appears to enhance its effectiveness. We proposed the structure-activity relationship of these compounds in natural products as a useful guide for developing new inhibitors of fungal activity.

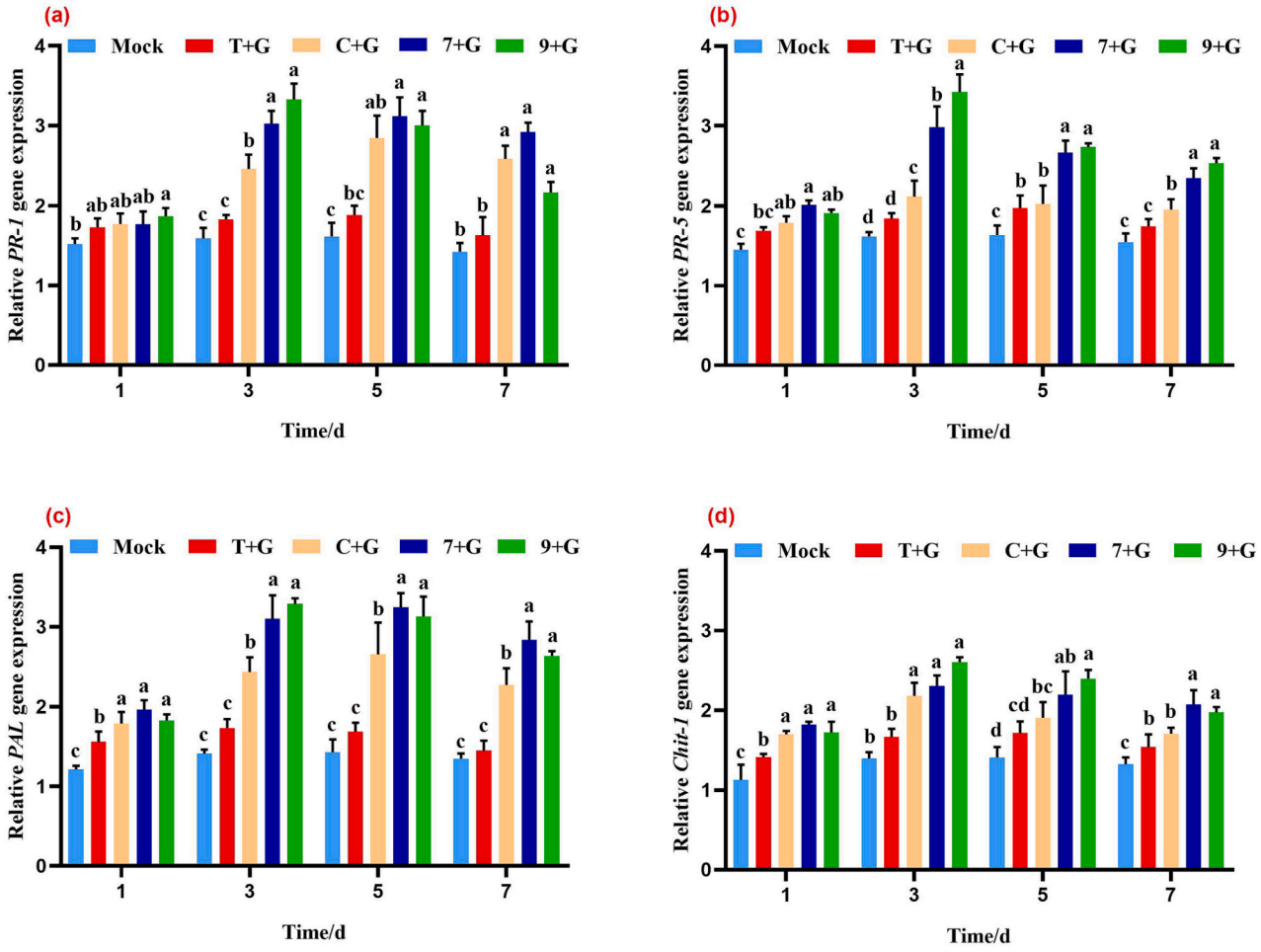

Fig. 8. Changes of transcriptional levels of *PR-1* (**a**), *PR-5* (**b**), *PAL* (**c**), and *Chit-1* (**d**) gene in tobacco leaves treated with 250 μg/mL of carbendazim, compounds **7** and **9**. Mock: healthy tobacco; T + G: *G. cichoracearum* in 0.1% of Tween-20 solution (negative control); C + G: treatment with carbendazim; **7** + G: treatment with **7**; **9** + G: treatment with **9**. All results were expressed as the average value of three measurements for all group.

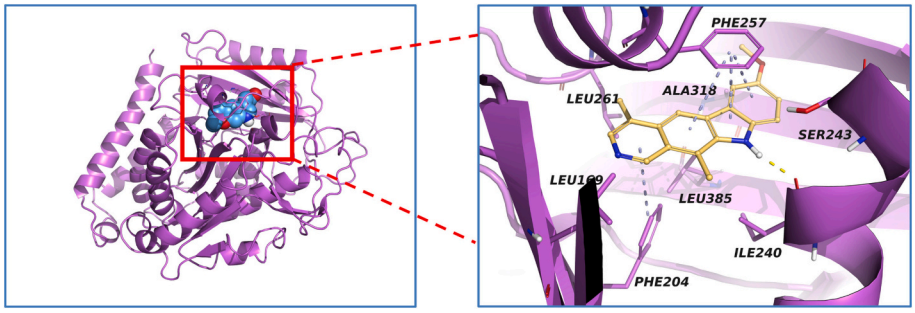

Fig. 9. Binding modes of compound **9** with tubulin (*G. cichoracearum*) protein. Key residues are represented as stick models; hydrogen bonds are depicted as dotted yellow lines and π–π stacking interaction is depicted as dotted blue line. (For interpretation of the references to color in this figure legend, the reader is referred to the web version of this article.)

4. Conclusion

Consequently, a total of 14 indole alkaloid derivatives were isolated from the fermented extract of *A. fumigatus* 0338. To our knowledge, compounds **1**–**3** represent rare linearly fused 6/6/5 tricyclic prenylated indole alkaloid. Isopentenyl substitutions at the 5-position found in compounds **4** and **5** are also uncommon. Compounds **6** and **7** feature novel indole alkaloid derivative skeletons.

The results of the anti-*G. cichoracearum* activity experiment showed that all compounds exhibited some level of activity, with compounds **7** and **9** showing the best results in terms of inhibition rate, protective effect, and curative effect. Observations of changes in the spores of *G. cichoracearum* on the leaf surface and leaf tissue structure after treatment with compound **9** revealed that it could directly target and destroy the spores of the *G. cichoracearum*, as well as restore leaf tissue characteristics to enhance plant resistance to pathogens. Additionally, compounds **7** and **9** could induce the activity of several defense-related enzymes (PAL, CAT and APX), plant hormones (SA, JA, MDA and CHL), and upregulate the expression of defense-related genes in tobacco leaves infected with powdery mildew, thereby stimulating SAR in plants and

enhancing their disease resistance capabilities. Molecular docking results indicated that the indole core structure in these compounds may be the basis for their anti-*G. cichoracearum* activity. The docking results, combined with the activity experiment results, demonstrated that compounds with the parental structure of **6**, **7** and **9** had better activity than the others. Among **6** and **7**, methoxy substitution could enhance their anti-*G. cichoracearum* activity. These compounds have the ability to activate innate disease resistance mechanisms within plants, and they can also directly act on the powdery mildew pathogen *G. cichoracearum*. To our knowledge, this is the first demonstration that these indole alkaloid derivatives, particularly **7** and **9**, have the potential to serve as inducers of plant SAR and novel plant protectants. The successful isolation and identification of these indole alkaloids, as well as the in-depth study of their anti-*G. cichoracearum* activity and mechanisms, provide valuable resources for the discovery of antifungal inhibitors. Moreover, these findings have made significant contributions to the development and utilization of microorganisms derived from tobacco.

CRediT authorship contribution statement

Yue-Yu Ma: Writing – review & editing, Methodology, Data curation. **Gui Pu:** Data curation. **Hua-Yin Liu:** Methodology. **Sui Yao:** Validation. **Guang-Hui Kong:** Formal analysis. **Yu-Ping Wu:** Investigation. **Yin-Ke Li:** Investigation. **Wei-Guang Wang:** Investigation. **Min Zhou:** Conceptualization. **Qiu-Fen Hu:** Supervision, Project administration, Funding acquisition, Conceptualization. **Feng-Xian Yang:** Supervision, Project administration, Funding acquisition, Conceptualization.

Declaration of competing interest

The authors declare that no competing interests exist.

Data availability

Data will be made available on request.

Acknowledgments

The National Natural Science Foundation of China (No. 21967021 and No. 32301271) provided financial support for this project, as did the Yunnan Tobacco Company Foundation (No. 2020530000241001 and 2021530000241002), the Yunnan Innovative Research Team Foundation (2019HC020) and the Yunnan Provincial Department of Education Science Research Fund Project (No. 2023Y0546).

Appendix A. Supplementary data

Supplementary data to this article can be found online at https://doi.org/10.1016/j.pestbp.2024.105814.

References

Abookleesh, F.L., Al-Anzi, B.S., Ullah, A., 2022. Potential antiviral action of alkaloids. Molecules 27 (3), 903. https://doi.org/10.3390/molecules27030903.

Amil-Ruiz, F., Garrido-Gala, J., Gadea, J., Blanco-Portales, R., Muñoz-Mérida, A., Trelles, O., de Los Santos, B., Arroyo, F.T., Aguado-Puig, A., Romero, F., Mercado, J.Á., Pliego-Alfaro, F., Muñoz-Blanco, J., Caballero, J.L., 2016. Partial activation of SA- and JA-defensive pathways in strawberry upon *Colletotrichum acutatum* interaction. Front. Plant Sci. 7, 1036. https://doi.org/10.3389/fpls.2016.01036.

Barber, A.E., Riedel, J., Sae-Ong, T., Kang, K., Brabetz, W., Panagiotou, G., Deising, H.B., Kurzai, O., 2020. Effects of agricultural fungicide use on *Aspergillus fumigatus* abundance, antifungal susceptibility, and population structure. MBio. 11 (6), e02213–e02220. https://doi.org/10.1128/mBio.02213-20.

Basaid, K., Chebli, B., Mayad, E.H., Furze, J.N., Bouharroud, R., Krier, F., Barakate, M., Paulitz, T., 2020. Biological activities of essential oils and lipopeptides applied to control plant pests and diseases: a review. Int. J. Pest Manag. 67 (2), 155–177. https://doi.org/10.1080/09670874.2019.1707327.

Beukes, D.R., Davies-Coleman, M.T., Kelly-Borges, M., Harper, M.K., Faulkner, D.J., 1998. Dilemmaones A-C, unusual indole alkaloids from a mixed collection of south African sponges. J. Nat. Prod. 61 (5), 699–701. https://doi.org/10.1021/np970580m.

Chen, H., Bai, J., Fang, Z.F., Yu, S.S., Ma, S.G., Xu, S., Li, Y., Qu, J., Ren, J.H., Li, L., Si, Y. K., Chen, X.G., 2011. Indole alkaloids and quassinoids from the stems of *Brucea mollis*. J. Nat. Prod. 74 (11), 2438–2445. https://doi.org/10.1021/np200712y.

Dai, J.M., Zhu, L.C., Xiao, D., Xie, J., Wang, X., Mi, Q.L., Shi, Q.J., Yin, G.Y., Yang, Y.K., Yang, G.Y., Hu, Q.F., Wang, K., 2022. Two new anthraquinones from the cigar tobacco-derived fungus *Aspergillus versicolor* and their bioactivities. Chem. Nat. Compd. 58, 1001–1005. https://doi.org/10.1007/s10600-022-03854-z.

Dai, J.M., Mi, Q.L., Li, X.M., Du, G., Yang, G.Y., Zhang, J.D., Wang, J., Li, Y.K., Yang, H. Y., Miao, D., Li, Z.J., Hu, Q.F., 2023. The anti-TMV potency of the tobacco-derived fungus *Aspergillus versicolor* and its active alkaloids, as anti-TMV activity inhibitors. Phytochemistry 205, 113485. https://doi.org/10.1016/j.phytochem.2022.113485.

Degenkolb, T., Vilcinskas, A., 2016. Metabolites from nematophagous fungi and nematicidal natural products from fungi as alternatives for biological control. Part II: metabolites from nematophagous basidiomycetes and non-nematophagous fungi. Appl. Microbiol. Biotechnol. 100 (9), 3813–3824. https://doi.org/10.1007/s00253-015-7234-5.

Dietz, K.J., Turkan, I., Krieger-Liszkay, A., 2016. Redox-and reactive oxygen species dependent signaling into and out of the photosynthesizing chloroplast. Plant Physiol. 171 (3), 1541–1550. https://doi.org/10.1104/pp.16.00375.

Dong, X., Zhao, Y., Ran, X., Guo, L.X., Zhao, D.G., 2017. Overexpression of a new chitinase gene EuCHIT2 enhances resistance to *Erysiphe cichoracearum* DC in tobacco plants. Int. J. Mol. Sci. 18 (11), 2361. https://doi.org/10.3390/ijms18112361.

Fujimoto, T., Abe, H., Mizukubo, T., Seo, S., 2021. Phytol, a constituent of chlorophyll, induces root-knot nematode resistance in *Arabidopsis* via the ethylene signaling pathway. Mol. Plant-Microbe Interact. 34 (3), 279–285. https://doi.org/10.1094/mpmi-07-20-0186-r.

Gamit, H.A., Naik, H., Chandarana, K.A., Chandwani, S., Amaresan, N., 2023. Secondary metabolites from methylotrophic bacteria: their role in improving plant growth under a stressed environment. Environ. Sci. Pollut. Res. Int. 30 (11), 28563–28574. https://doi.org/10.1007/s11356-023-25505-8.

Glawe, D.A., 2008. The powdery mildews: a review of the world's most familiar (yet poorly known) plant pathogens. Annu. Rev. Phytopathol. 46, 27–51. https://doi.org/10.1146/annurev.phyto.46.081407.104740.

Gullner, G., Juhász, C., Németh, A., Barna, B., 2017. Reactions of tobacco genotypes with different antioxidant capacities to powdery mildew and tobacco mosaic virus infections. Plant Physiol. Biochem. 119, 232–239. https://doi.org/10.1016/j.plaphy.2017.09.003.

Guo, Y., Dong, Y., Xu, C., Xie, Q., Xie, Y.B., Xia, Z.H., An, M.N., Wu, Y.H., 2020a. N-ovel combined biological antiviral agents cytosinpeptidemycin and chitosan oligosaccharide induced host resistance and changed movement protein subcellular localization of tobacco mosaic virus. Pestic. Biochem. Physiol. 164, 40–46. https://doi.org/10.1016/j.pestbp.2019.12.006.

Guo, Y.W., Liu, X.J., Yuan, J., Li, H.J., Mahmud, T., Hong, M.J., Yu, J.C., Lan, W.J., 2020b. L-tryptophan induces a marine-derived *Fusarium* sp. to produce indole alkaloids with activity against the *Zika* virus. J. Nat. Prod. 83 (11), 3372–3380. https://doi.org/10.1021/acs.jnatprod.0c00717.

Guo, W.L., Yang, H.L., Zhao, J.P., Bian, S.J., Guo, Y.Y., Chen, X.L., Li, X.Z., 2023. A pathogenesis-related protein 1 of *Cucurbita moschata* responds to powdery mildew infection. Front. Genet. 14, 1168138. https://doi.org/10.3389/fgene.2023.1168138.

Hagag, A., Abdelwahab, M.F., Abd El-Kader, A.M., Fouad, M.A., 2022. The endophytic *Aspergillus* strains: a bountiful source of natural products. J. Appl. Microbiol. 132 (6), 4150–4169. https://doi.org/10.1111/jam.15489.

Hu, Q.F., Ma, Y.Y., Liu, H.Y., Dai, J.M., Yang, F.X., Zhang, J.D., Wang, J., Li, X.M., Liu, X., Li, J., Li, Y.K., Wang, W.G., Zhou, M., Yang, G.Y., 2022. Antivirus isoindolinone alkaloids with rare oxocyclopenta*[f]*isoindole frameworks isolated from the stems of flue cured tobacco. Chem. Biol. Technol. Agric. 9, 88. https://doi.org/10.1186/s40538-022-00339-7.

Jiao, J., Gai, Q.Y., Wang, W., Zang, Y.P., Niu, L.L., Fu, Y.J., Wang, X., 2018. Remarkable enhancement of flavonoid production in a co-cultivation system of *Isatis tinctoria* L. hairy root cultures and immobilized *Aspergillus niger*. Ind. Crop. Prod. 112, 252–261. https://doi.org/10.1016/j.indcrop.2017.12.017.

Jiménez-Reyes, M.F., Carrasco, H., Olea, A.F., Silva-Moreno, E., 2019. Natural compounds: a sustainable alternative for controlling phytopathogens. J. Chil. Chem. Soc. 64 (2), 4459–4465. https://doi.org/10.4067/s0717-97072019000204459.

Kim, Y.B., Kim, S.M., Sathasivam, R., Kim, Y.K., Park, S.U., Kim, S.U., 2021. Overexpression of *Ginkgo biloba* hydroxy-2-methyl-2-(*E*)-butenyl-4-diphosphate reductase 2 gene (*GbHDR2*) in *Nicotiana tabacum* cv. Xanthi. 3 Biotech. 11, 337. https://doi.org/10.1007/s13205-021-02887-5.

Kong, L.W., Qiu, W.Y., Chen, M.S., Yang, W.L., Shen, J.R., Tang, X.B., He, X.H., Li, Y.K., Hu, Q.F., Kong, G.H., 2023. Two new antifungal indole alkaloids from an endophytic fungi *Aspergillus felis* obtained from cigar tobacco. Chem. Nat. Compd. 59, 1132–1136. https://doi.org/10.1007/s10600-023-04210-5.

Kwon, O.S., Ahn, S., Jeon, J.E., Park, I.G., Won, T.H., Sim, C.J., Park, H.G., Oh, D.C., Oh, K.B., Noh, M., Shin, J.H., 2021. Psammocindoles a-c: isolation, synthesis, and bioactivity of indole-γ-lactams from the sponge *Psammocinia vermis*. Org. Lett. 23 (12), 4667–4671. https://doi.org/10.1021/acs.orglett.1c01410.

Li, H.Q., Xu, D., Sun, W.G., Yang, B.Y., Li, F.L., Liu, M.T., Wang, J.P., Xue, Y.B., Hu, Z.X., Zhang, Y.H., 2019. HPLC–DAD–directed isolation of linearly fused prenylated indole alkaloids from a soil-derived *Aspergillus versicolor*. J. Nat. Prod. 82 (8), 2181–2188. https://doi.org/10.1021/acs.jnatprod.9b00183.

Lim, G.H., Shine, M.B., De Lorenzo, L., Yu, K., Cui, W., Navarre, D., Hunt, A.G., Lee, J.Y., Kachroo, A., Kachroo, P., 2016. Plasmodesmata localizing proteins regulate transport and signaling during systemic acquired immunity in plants. Cell Host Microbe 19 (4), 541–549. https://doi.org/10.1016/j.chom.2016.03.006.

Liu, L., Song, C.W., Khan, A., Li, X.N., Yang, X.W., Cheng, G.G., Liu, Y.P., Luo, X.D., 2016. A potent antibacterial indole alkaloid from *Psychotria pilifera*. J. Asian Nat. Prod. Res. 18 (8), 798–803. https://doi.org/10.1080/10286020.2016.1158710.

Liu, J., Chang, M.C., Meng, J.L., Liu, J.Y., Cheng, Y.F., Feng, C.P., 2020a. Effect of ozone treatment on the quality and enzyme activity of *Lentinus edodes* during cold storage. J. Food Process. Preserv. 44 (8), e14557 https://doi.org/10.1111/jfpp.14557.

Liu, Y., Cui, Y., Lu, L.Y., Gong, Y.F., Han, W., Piao, G.S., 2020b. Natural indole-containing alkaloids and their antibacterial activities. Arch. Pharm. (Weinheim). 353 (10), 2000120. https://doi.org/10.1002/ardp.202000120.

Ma, Y.Y., Xiong, W., Shen, S.Y., Li, S.S., Liu, X.S., Li, Y.K., Dong, M., Zhou, M., Wang, W. G., Du, G., Hu, Q.F., Ma, X.W., 2023. Bioactive indole alkaloids from the tobacco-derived endophytic fungus *Aspergillus fumigatus*. Chem. Nat. Compd. 59 (3), 524–528. https://doi.org/10.1007/s10600-023-04041-4.

Möller, P.A., Aucique-Pérez, C.E., Einhardt, A.M., Lemos, D.C., Rodrigues, F.Á., Badel, J. L., 2020. Impairment of photosynthetic capacity and hydrogen peroxide removal in *Castor bean* affected by bacterial leaf spot. Physiol. Mol. Plant P. 111, 101510. https://doi.org/10.1016/j.pmpp.2020.101510.

Obydennov, K.L., Kalinina, T.A., Galieva, N.A., Beryozkina, T.V., Zhang, Y., Fan, Z., Glukhareva, T.V., Bakulev, V.A., 2021. Synthesis, fungicidal activity, and molecular docking of 2-acylamino and 2-thioacylamino derivatives of 1*H*-benzo[*d*]imidazoles as anti-tubulin agents. J. Agric. Food Chem. 69 (40), 12048–12062. https://doi.org/10.1021/acs.jafc.1c03325.

Pathak, R., Ergon, Å., Stensvand, A., Gislerød, H.R., Solhaug, K.A., Cadle-Davidson, L., Suthaparan, A., 2020. Functional characterization of *Pseudoidium neolycopersici* photolyase reveals mechanisms behind the efficacy of nighttime UV on powdery mildew suppression. Front. Microbiol. 11, 1091. https://doi.org/10.3389/fmicb.2020.01091.

Peng, Y.J., Yang, J.F., Li, X., Zhang, Y.L., 2021. Salicylic acid: biosynthesis and signaling. Annu. Rev. Plant Biol. 72, 761–791. https://doi.org/10.1146/annurev-arplant-081320-092855.

Quaglia, M., Fabrizi, M., Zazzerini, A., Zadra, C., 2012. Role of pathogen-induced volatiles in the *Nicotiana tabacum-Golovinomyces cichoracearum* interaction. Plant Physiol. Biochem. 52, 9–20. https://doi.org/10.1016/j.plaphy.2011.11.006.

Rienth, M., Crovadore, J., Ghaffari, S., Lefort, F., 2019. Oregano essential oil vapour prevents *Plasmopara viticola* infection in grapevine (*Vitis Vinifera*) and primes plant immunity mechanisms. PLoS One 14 (9), e0222854. https://doi.org/10.1371/journal.pone.0222854.

Sachse, C., Chen, J.Z., Coureux, P.D., Stroupe, M.E., Fändrich, M., Grigorieff, N., 2007. High-resolution electron microscopy of helical specimens: a fresh look at tobacco mosaic virus. J. Mol. Biol. 371 (3), 812–835. https://doi.org/10.1016/j.jmb.2007.05.088.

Schmidt, U., Theumer, G., Jäger, A., Kataeva, O., Wan, B., Franzblau, S.G., Knölker, H.J., 2018. Synthesis and activity against *Mycobacterium tuberculosis* of olivacine and oxygenated derivatives. Molecules 23 (6), 1402. https://doi.org/10.3390/molecules23061402.

Shi, L.J., Wu, Y.M., Yang, X.Q., Xu, T.T., Yang, S., Wang, X.Y., Yang, Y.B., Ding, Z.T., 2020. The cocultured *Nigrospora oryzae* and *Collectotrichum gloeosporioides*, *Irpex lacteus*, and the plant host *Dendrobium officinale* bidirectionally regulate the production of phytotoxins by anti-phytopathogenic metabolites. J. Nat. Prod. 83 (5), 1374–1382. https://doi.org/10.1021/acs.jnatprod.0c00036.

Singh, T.P., Singh, O.M., 2018. Recent progress in biological activities of indole and indole alkaloids. Mini-Rev. Med. Chem. 18 (1), 9–25. https://doi.org/10.2174/1389557517666170807123201.

Singh, R.R., Chinnasri, B., De Smet, L., Haeck, A., Demeestere, K., Van Cutsem, P., Van Aubel, G., Gheysen, G., Kyndt, T., 2019. Systemic defense activation by COS-OGA in rice against root-knot nematodes depends on stimulation of the phenylpropanoid pathway. Plant Physiol. Biochem. 142, 202–210. https://doi.org/10.1016/j.plaphy.2019.07.003.

Tabassum, F., Hasan, C.M., Masud, M.M., Jamshidi, S., Rahman, K.M., Ahsan, M., 2021. Indole alkaloids from the leaves of *Ravenia spectabilis engl*. With activity against pancreatic cancer cell line. Phytochemistry 186, 112744. https://doi.org/10.1016/j.phytochem.2021.112744.

Wang, H.C., Li, W.H., Xia, H.Q., Wang, M.S., Meng, L., Shi, J.X., Sheng, S.H., Wang, J.G., 2012a. Toxicity and control efficacy of azoxystrobin and pyraclostrobin against *Erysiphe cichoracearum* on tobacco during seedling developing period. Chin. J. Pestic. Sci. 14 (4), 412–416. https://doi.org/10.3969/j.issn.1008-7303.

Wang, H.C., Yang, S.J., Xu, D.Q., Chen, X.J., Hu, X.D., Shang, S.H., Shi, J.X., 2012b. Fungicidal activity of benzothiadiazole to *Erysiphe cichoracearum* and its safety to tobacco seedlings. Chin. J. Plant Prot. 38 (6), 123–126. https://doi.org/10.3969/j.issn.0529–1542.

Xing, H.H., Liang, C., Yu, J., Zhang, C.S., Kong, F.Y., Wang, F.L., 2015. Biological characteristics of tobacco powdery mildew pathogen. Acta Tabacaria Sinica 21 (2), 85–89. https://doi.org/10.16472/j.chinatobacco.2014.050.

Yan, H., Li, Q., Park, S.C., Wang, X., Liu, Y.J., Zhang, Y.G., Tang, W., Kou, M., Ma, D.F., 2016. Overexpression of CuZnSOD and APX enhance salt stress tolerance in sweet potato. Plant Physiol. Biochem. 109, 20–27. https://doi.org/10.1016/j.plaphy.2016.09.003.

Yan, Y., Wang, D., Zhang, X., Peng, M.Y., Yan, X.Y., Guo, Y.S., Jia, M.G., Zhou, J., Tang, L., Hao, X.J., 2022. Anti-TMV activity and effects of three prieurianin-type limonoids from *Munronia henryi*. Pestic. Biochem. Physiol. 184, 105108 https://doi.org/10.1016/j.pestbp.2022.105108.

Yang, T., Zhu, L.S., Meng, Y., Lv, R., Zhou, Z., Zhu, L., Lin, H.H., Xi, D.H., 2018. Alph-amomorcharin enhances tobacco mosaic virus resistance in tobacco^{NN} by manipulating jasmonic acid-salicylic acid crosstalk. J. Plant Physiol. 223, 116–126. https://doi.org/10.1016/j.jplph.2017.04.011.

Yang, G.Y., Dai, J.M., Mi, Q.L., Wang, J., Yang, F.X., Liu, X., Li, J., Gao, Q., Li, X.M., Li, Y. K., Wang, W.G., Zhou, M., Hu, Q.F., 2022. Cyclopiazonic acid type indole alkaloids from *Nicotiana tabacum*-derived fungus *Aspergillus versicolor* and their anti-tobacco mosaic virus activities. Phytochemistry 198, 113137. https://doi.org/10.1016/j.phytochem.2022.113137.

Yang, F.X., Dai, J.M., Liu, H.Y., Mi, Q.L., Wang, J., Zhang, J.D., Li, X.M., Wang, W.G., Zhou, M., Li, Y.K., Hu, Q.F., 2023a. Isochromenes from the *Nicotiana tabacum*-derived endophytic fungus *Aspergillus versicolor* and their anti-tobacco mosaic virus activities. Nat. Prod. Res. 37 (10), 1608–1616. https://doi.org/10.1080/14786419.2022.2103554.

Yang, H.J., Peng, L.Y., Li, Z.M., Huang, C.Y., Huang, J.G., 2023b. Biocontrol of *Lysobacter enzymogenes* CQ18 against the tobacco powdery mildew fugus, *Erysiphe cichoracearum*. Chem. Biol. Technol. Agric. 10, 74. https://doi.org/10.1186/s40538-023-00436-1.

Zhang, J., Wang, J.D., Liu, C.X., Yuan, J.H., Wang, X.J., Xiang, W.S., 2014. A new prenylated indole derivative from endophytic actinobacteria *Streptomyces* sp. NEAU-D50. Nat. Prod. Res. 28 (7), 431–437. https://doi.org/10.1080/14786419.2013.871546.

Zhao, L.H., Dong, J.H., Hu, Z.T., Li, S.L., Su, X.X., Zhang, J., Yin, Y.Y., Xu, T., Zhang, Z.K., Chen, H.R., 2017. Anti-TMV activity and functional mechanism of two sesquiterpenoids isolated from *Tithonia diversifolia*. Pestic. Biochem. Physiol. 140, 24–29. https://doi.org/10.1016/j.pestbp.2017.05.009.

Zhou, M., Lou, J., Li, Y.K., Wang, Y.D., Zhou, K., Ji, B.K., Dong, W., Gao, X.M., Du, G., Hu, Q.F., 2015a. Butyrolactones from the endophytic fungus *Aspergillus versicolor* and their anti-tobacco mosaic virus activity. J. Braz. Chem. Soc. 26 (3), 545–549. https://doi.org/10.5935/0103-5053.20150008.

Zhou, M., Du, G., Yang, H.Y., Xia, C.F., Yang, J.X., Ye, Y.Q., Gao, X.M., Li, X.N., Hu, Q.F., 2015b. Antiviral butyrolactones from the endophytic fungus *Aspergillus versicolor*. Planta Med. 81 (3), 235–240. https://doi.org/10.1055/s-0034-1396153.

Zhou, M., Zhou, K., He, P., Wang, K.M., Zhu, R.Z., Wang, Y.D., Dong, W., Li, G.P., Yang, H.Y., Ye, Y.Q., Du, G., Li, X.M., Hu, Q.F., 2016. Antiviral and cytotoxic isocoumarin derivatives from an endophytic fungus *Aspergillus oryzae*. Planta Med. 82 (5), 414–417. https://doi.org/10.1055/s-0035-1558331.